Energy Yield Analysis of Multiterminal Si-Based Tandem Solar Cells

Henning Schulte-Huxel, Timothy J. Silverman, Michael G. Deceglie, Daniel J. Friedman, and Adele C. Tamboli

***Abstract*—We present a model for a yield analysis of tandem devices consisting of Si bottom cells with III-V top cells. It accounts for the spectral properties of the subcells as well as their reduced operating temperature due to increased efficiency and luminescent coupling. Inputs are the experimental *I–V* and QE data of the subcells (e.g., available from laboratory prototypes) and the irradiance-dependent module temperature of the bottom cell. We apply the model to compare two types of tandem cells, GaInP and GaAs top cells on Si bottom cells. The impact of the temperature model, compared to a constant temperature, shows a relative change in energy yield of up to 2.7%$_{rel}$. Including luminescent coupling for GaAs/Si devices with two terminals, increases the energy yield by 34.0%$_{rel}$. This is still 34.2%$_{rel}$ less energy yielded than for GaInP/Si two-terminal devices. The performance of the GaInP/Si devices can be improved by 5.8%$_{rel}$ using three-terminal devices with back-contacted bottom cells instead of a two-terminal configuration under the assumption of a cell string with voltage matching of one top cell with two bottom cells. For GaInP/Si, the three-terminal device performs similarly to the four-terminal device, enabling the integration of monolithic tandem cells into modules at comparably high efficiencies.**

***Index Terms*—Energy yield calculations, luminescent coupling, Si-based tandem solar cells.**

I. Introduction

TANDEM solar cells with Si bottom cells for terrestrial non-concentrator applications have shown increasing promise in recent years due to their demonstrated efficiencies exceeding the theoretical limit of single-junction solar cells. Tandem cells have reached efficiency records of over 32% [1] with III-V top cells based on GaAs and GaInP and 26% with perovskite top cells [2]. In addition to the material combination, the design of the subcells and the bonding technique have a large impact on the device performance. Various subcell interconnection configurations of the tandem cells are possible, i.e., a tandem cell featuring two, three, or four terminals [3], [4].

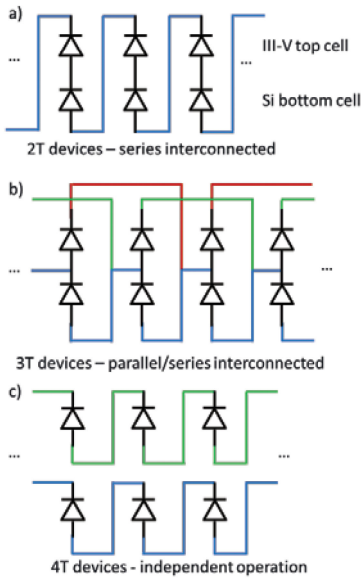

Fig. 1. Schemes of the interconnection of (a) 2T, (b) 3T, and (c) 4T tandem cells. 2T devices are limited by current matching of the subcells, and interconnected 3T devices are limited by matching of the voltages in the substrings of top and bottom cells. These configurations are described in more detail in [4].

Two-terminal (2T) devices have the advantage that for module integration, they can be interconnected in series, as with single junction devices [see Fig. 1(a)]. However, series interconnection requires current matching of the subcells. This current matching results in a strong restriction of the bandgap of the top cell and may cause significant performance losses under varying spectra [3]–[6]. Operating the two subcells independently, as in the case of four-terminal (4T) devices [3], [6], [7], circumvents the current matching constraint, as shown in Fig. 1(c). However, this results in a more complex system integration. Part of the mismatch losses in case of 2T devices can be recovered by luminescent coupling [8], [9], if the bottom cell is the current-limiting device.

Device modeling has predicted that three-terminal (3T) devices perform the same as 4T devices, and the effects on the device performance due to extracting power from the two different subcircuits of the bottom cell are marginal [10], [11]. 3T

Manuscript received March 18, 2018; revised May 17, 2018; accepted June 3, 2018. Date of publication July 6, 2018; date of current version August 20, 2018. The work of H. Schulte-Huxel was supported by the Research Fellowship by Deutsche Forschungsgemeinschaft Grant SCHU 3206/1-1. This work was supported by the Alliance for Sustainable Energy, LLC, the manager and operator of the National Renewable Energy Laboratory for the U.S. Department of Energy under Contract DE-AC36-08GO28308. This work was also supported by the U.S. Department of Energy Office of Energy Efficiency and Renewable Energy Solar Energy Technologies Office under Contract DE-EE00030299. *(Corresponding author: Henning Schulte-Huxel.)*

H. Schulte-Huxel was with the National Renewable Energy Laboratory, Golden, CO 80401 USA. He is now with the Institute for Solar Energy Research Hamelin, 31860 Emmerthal, Germany (e-mail: h.schulte@isfh.de).

T. J. Silverman, M. G. Deceglie, D. J. Friedman, and A. C. Tamboli are with the National Renewable Energy Laboratory, Golden, CO 80401 USA (e-mail: Timothy.Silverman@nrel.gov; Michael.Deceglie@nrel.gov; Daniel.Friedman@nrel.gov; Adele.Tamboli@nrel.gov).

Color versions of one or more of the figures in this paper are available online at http://ieeexplore.ieee.org.

Digital Object Identifier 10.1109/JPHOTOV.2018.2846520

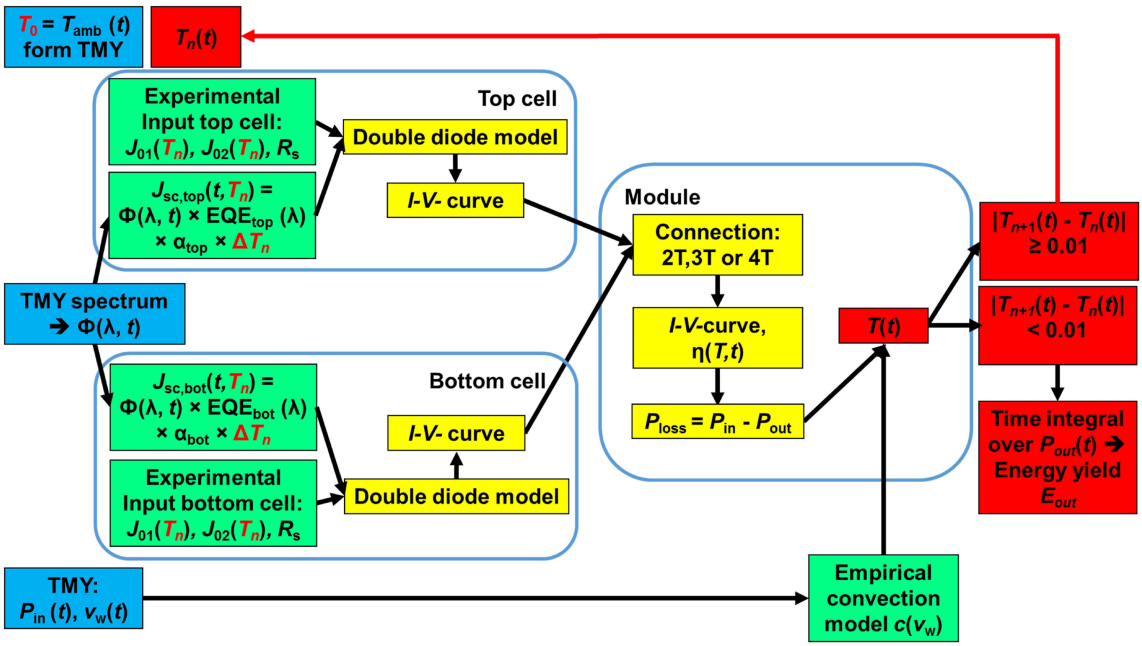

Fig. 2. Scheme of the applied model to calculate the energy yield of novel tandem modules using TMY data [ambient temperature T_{amb}, wind speed v_w, total irradiance ($\hat{=}P_{in}$), and spectral irradiance to calculate the spectral photon flux $\Phi(\lambda)$]. Experimental inputs are the double diode model saturation current densities J_{01} and J_{02}, *EQE*, series resistances R_s and linear temperature coefficient α of the current for each subcell and an empirical model with $c(v_w)$ comprising the thermal convection and subband gap radiation properties of the module. The operating temperature T is determined iteratively.

devices can also have benefits in cell processing and interconnection compared to 4T devices. For example, Si cells with an interdigitated back contact (IBC) design and a conductive front surface field can be used to enable tandem cells that do not require intermediate grids [12].

For the use of 3T devices in modules, the devices need to be interconnected appropriately, which adds significant restrictions to the operation of the devices compared to the operation as a single device. One interconnection method is in a combined parallel/series scheme [3], [4], [13], as shown in Fig. 1(b). This requires that the voltages of more than one series-connected bottom cell (e.g., two) are matched with the voltage of one parallel-connected top cell. This interconnection scheme is independent of the type of 3T device, e.g., if the third contact is enabled by the IBC bottom cell or if the cells feature a middle contact etched through one junction [14]. It was shown that this voltage matching is more robust against spectral changes than current matching [3], [4], [15], [16], which is beneficial for the energy yield [17].

Yield analysis is crucial to evaluating the potential and costs of new photovoltaic (PV) technologies in different configurations. Outdoor performance data from the final device are necessary for a justified yield analysis. However, such data are not available for new technologies, since often only a limited number of sensitive, small-scale laboratory devices are available. However, their experimental *I–V* and QE data are available. Thus, a simple model based on experimental input data to determine the energy yield of such novel devices is needed.

In many theoretical studies analyzing the energy yield under global spectra, only spectral data are taken into account for the yield analysis, and temperature effects are neglected [18] or estimated by an elevated constant temperature [19]. More detailed works [20] use well proven and widely used temperature models based on empirical data of existing modules from, for example, King *et al*. [21], but these models might underestimate the performance of new technologies. For example, less heat may be generated due to less thermalization, resulting from higher efficiency or less absorption of sub-bandgap light. Other works use a constant relation between irradiance and temperature increase independent of cell efficiency and wind speed [17], [22] for the comparison of different technologies. New models for energy yield of tandem devices [23], [24] take into account the effect of increased efficiency, but neglect wind speed and, like the works mentioned above, also neglect luminescent coupling. Alternatively, physical models to determine the operating temperature are available [25], [26] that thoroughly consider the thermal aspects of new modules. However, they require detailed characterization of all module components and sophisticated simulations.

The approach used here accounts for the power received and the power delivered by the PV module. It includes the electrical power output as a function of spectral irradiance and temperature, as well as radiation and convection interpolated from existing outdoor performance measurements of a module with a similar bottom cell. These data are then corrected by the enhanced energy conversion of the incoming light resulting in less heating of the module. With this model, we are able to predict the annual yield of new module technologies by taking into account the interdependencies between light absorption, module operating temperature and energy conversion efficiency, and account for meteorological conditions.

In this paper, we analyze the implications of the model, focusing on thermal and spectral effects as well as luminescent coupling. We consider two different combinations of tandem devices, a GaAs/Si device with a current-limiting top junction and a GaInP/Si device with a current-limiting bottom junction, as well as several different device configurations (2T, 3T, and 4T).

II. Model

The model presented in this paper is schematically shown in Fig. 2. It requires as input parameters 1) meterological data, which include spectral irradiance E, ambient temperature T_{amb}, and wind speed v_{w}, 2) experimental data of each subcell of the tandem device under standard testing conditions (STC) to extract the double diode model saturation current densities J_{01} and J_{02}, external quantum efficiency (EQE), series resistances R_{s}, and the temperature coefficient of the short circuit current density J_{sc}, as well as 3) an empirical convection factor $c(v_{\mathrm{w}})$ of a module with similar bottom cells in order to include the impact of irradiation and wind speed on the operation temperature T. The cell parameters are given in Table I and the EQE of the subcells in Fig. 7.

As meterological input parameters, we use typical meteorological year (TMY) data with a time resolution of 1 h for spectral and total irradiance, wind speed and outdoor temperature, in Denver, CO, USA (39.73°N, 104.74°W) [27].

For every hour of the year and for every tandem configuration, we calculate the spectral photon flux $\Phi(\lambda)$ based on the spectral irradiance and, using the EQE of the subcells, calculate the short circuit current density J_{sc} for each junction. Additional optical effects are neglected for simplicity. The experimental EQE data for all subcells are taken from [1]. The temperature dependence of the short circuit current density J_{sc} is taken into account by the linear coefficient α [28]–[30]; α_{bot} of the bottom cell is corrected for the effects of increased absorption in the top cells due to temperature-dependent bandgap shifts as taken into account by α_{top}. We describe the *I–V* curve and operation of the subcells by the double diode model. We extract the parameters for the double diode model under STC by interpolation from experimentally measured *I–V* curves of Si cells [31] and of GaAs and GaInP cells [1]. Since the shunt resistances of all investigated subcells are higher than 10 kΩ cm², the impact of the shunt resistance is neglected.

The temperature dependences of the saturation current densities $J_{01}(T)$ and $J_{02}(T)$ are implemented according to [32]

$$J_{01}(T) \propto T^3 e^{-E_{\mathrm{g}}/kT} \tag{1}$$

$$J_{02}(T) \propto T^{5/2} e^{-E_{\mathrm{g}}/2kT} \tag{2}$$

with the temperature dependent bandgap E_{g} (here used from [33]–[35]), and k is the Boltzmann constant.

Based on the *I–V* curves of the subcells, we calculate the *I–V* curves of the devices interconnected in strings. In the case of a 2T tandem solar cell, the top and bottom subcells are series connected on the cell as well as on the module level, as shown in Fig 1(a). Therefore, we add the voltages of the top and bottom subcells' *I–V* curves for equal currents in order to extract the temperature-dependent efficiency $\eta(T)$ at the maximum power point of the resultant *I–V* curves. For 3T devices, we only take the most relevant case of one top subcell in parallel to two bottom subcells [3], [4] into account, as shown in Fig. 1(b). Thus, we calculate the *I–V* curve and $\eta(T)$ of a string of 3T cells by adding the currents of the top J_{top} and bottom subcells J_{bot} for $V_{\mathrm{top}}(J_{\mathrm{top}}) = 2\,V_{\mathrm{bot}}(J_{\mathrm{bot}})$. Additional losses at the string ends [3] and due to minor effects occurring in the operation of 3T bottom cell are neglected [10], [11]. For the independent operation of the subcells in 4T devices and their strings as shown in Fig. 1(c), we sum up the power at maximum power point P_{mpp} of the individual subcells.

TABLE I
Double Diode Model Parameters Extracted From Experimental Data of Each Subcell of the Tandem Device Under STC

	GaAs	GaInP	Si
J_{01} [A/cm²]	7.86×10^{-21}	3.03×10^{-27}	18.15×10^{-15}
J_{02} [A/cm²]	3.42×10^{-12}	2.20×10^{-15}	3.556×10^{-9}
R_{s} [Ω cm²]	0.718	1.363	0.441
α [%/K]	0.066	0.075	0.045

The ideality factors for the double diode model are $n_1 = 1$ and $n_2 = 2$. J_{01} and J_{02} are the saturation current densities, R_{s} the series resistances, and α the linear temperature coefficient of the short circuit current.

The temperature of a module is determined based upon total incoming energy P_{in} reduced by the energy delivered by the module as the power output $P_{\mathrm{out}} = P_{\mathrm{in}} \times \eta(T)$, which generates no heat in the module as in the approach by Hove [36]. Compared to single-junction modules, P_{out} is significantly higher due to reduced thermalization losses, which reduces the module temperature. Here, we consider the thermal exchange of the module with its surroundings using outdoor performance data of a silicon PV module. Thereby, we include the convective and radiative properties of the module encapsulation, under the assumption that future tandem modules are encapsulated in the same way as current single-junction modules. Additionally, the module's reflection, especially the sub-bandgap reflection of the bottom cell, is considered, because the top cell transmits nearly all IR light and thus has negligible effect of the IR absorption.

We determine the module temperature as a function of wind speed, outdoor temperature, and irradiance using experimental data from a module with back-contacted Si solar cells located at the outdoor test field at NREL, Golden, CO, USA. Modules face south and have a tilt of 40°, which we also assume for the simulation. These modules have IR radiation and convective properties very similar to the ones we aim to predict. The data were collected over one year with data acquisition every minute. We ignore data for irradiance below 10 W/m² in order to focus on the module temperature during operation. Based on the known module efficiencies and temperature coefficients of the module, we convert the incident irradiance P_{in} to the loss power density

$$P_{\mathrm{loss}} = P_{\mathrm{in}} - P_{\mathrm{out}} = P_{\mathrm{in}} \times (1 - \eta(T)). \tag{3}$$

Fig. 3(a) and (b) shows the difference between ambient and module temperature ΔT of the module as the function of P_{loss} for

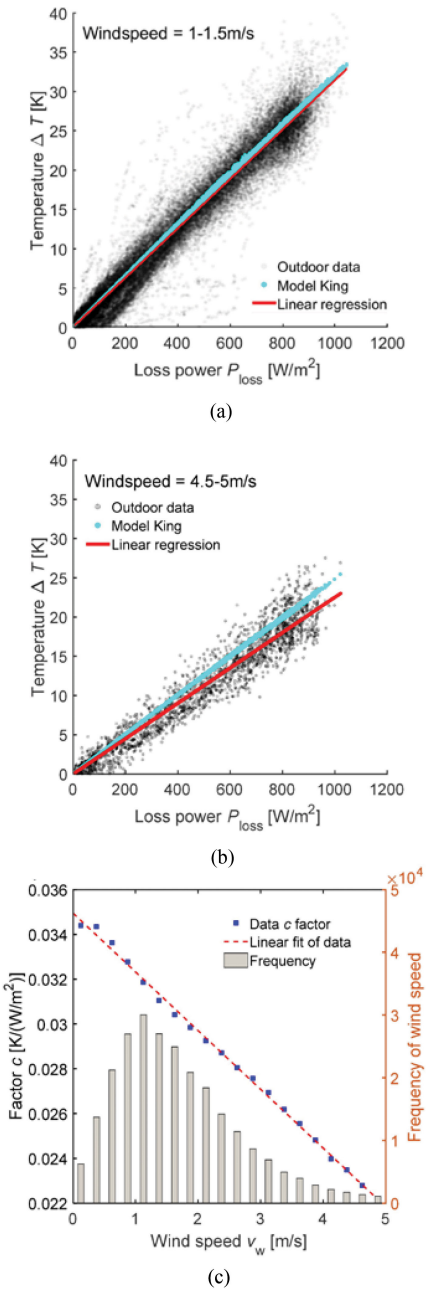

Fig. 3. (a) and (b) Si module temperature's deviation from ambient temperature, ΔT, as function of P_{loss} for two different wind speed ranges. The grey dots correspond to the measured data, the blue dots correspond to the model of King *et al*. [21] and the red lines are linear regressions. For this Si module, the King model and linear regression of our model agree well. However, for increasing wind speed, the King model overestimates the module temperature. (c) The proportionality factor c of the linear regressions (blue symbols) as function of wind speed v_{w} and their linear fit (red dashed line). Additionally, the frequency of the wind speeds for the time of data acquisition (whole year 2016 at the outdoor test field at NREL, Golden, CO, USA).

two different wind speeds v_{w}. We observe a linear correlation between P_{loss} and ΔT, as is also predicted by the model of King *et al.* [21]. Since the temperature of the module follows an increase of irradiance and ambient temperature with some delay due to the module's nonzero heat capacity, the thermal history is included by a moving average over 12 min, which showed the lowest norm of residuals for the linear fits. This satisfactorily predicts the temperature increase without separate consideration of radiative heat transfer effects. The slope of the linear regression (red lines) is affected by the wind speed. Therefore, we describe ΔT for a certain wind speed v_{w} by

$$\Delta T = c\,(v_w)\,P_{\text{loss}}\,(\eta, T) \tag{4}$$

with the wind dependent convection factor $c(v_{\text{w}})$. Fig. 3(c) shows $c(v_{\text{w}})$ as a function of v_{w} (blue symbols), indicating a linear dependence. As a consequence, we describe $c(v_{\text{w}})$ in case of the investigated module by

$$c = 0.0349\ \text{K m s /W}\ \times v_w - 0.00262\ \text{K m}^2\text{/W}. \tag{5}$$

According to (3) and (4), the module efficiency influences the module temperature. The temperature-dependent efficiency and the resulting operation temperature is calculated iteratively until the temperature difference between two iterations is below 0.01 K. We start the iteration with ambient temperature. We assume a homogeneous temperature within the module, and in particular, the same temperature for both subcells.

For series-connected subcells (2T), the top and bottom bandgaps may not be matched perfectly, and luminescent coupling may need to be taken into account. In case of the GaAs/Si tandem devices, the bottom cell is the current-limiting cell. Thus, the top cell operates near open circuit condition and emits photons because of the radiative recombination. These can be absorbed by the bottom cell. Thus, this luminescent coupling increases J_{bot} and decreases current mismatch losses. To investigate this effect, we calculate the current enhancement for the bottom cell ΔJ because of the luminescence from the forward-biased top cell, according to [8]

$$\Delta J_{\text{bot}}\left(V_{\text{top}}, T\right) = \eta_{\text{LC}} \times J_{01\text{top}}\left(V_{\text{top}}, T\right) \tag{6}$$

with η_{LC} the luminescent coupling constant and $J_{01top}(V_{\text{top}}, T)$ the saturation current density of the top cell, which depends on the top cell's voltage and temperature.

As described above, we calculate the current based on the EQE, i.e., the active cell area without encapsulation. In a module, the current density J would be reduced by inactive areas, absorption, and reflection. The reflection of the module depends highly on the cells' dimension, metallization, and interconnection scheme, which are difficult to predict and have only small effects on the relative current yield between the different technologies. The same applies for series resistance contributions because of the interconnections. Thus, these factors are neglected here. However, the absorption by the encapsulation has a significant effect on the spectrum and is investigated here by using the absorption of a 450-μm-thick layer of ethylene-vinyl acetate (EVA) with enhanced transmission and a 4-mm-thick layer of low iron glass, as simulated using their extinction coefficients [37].

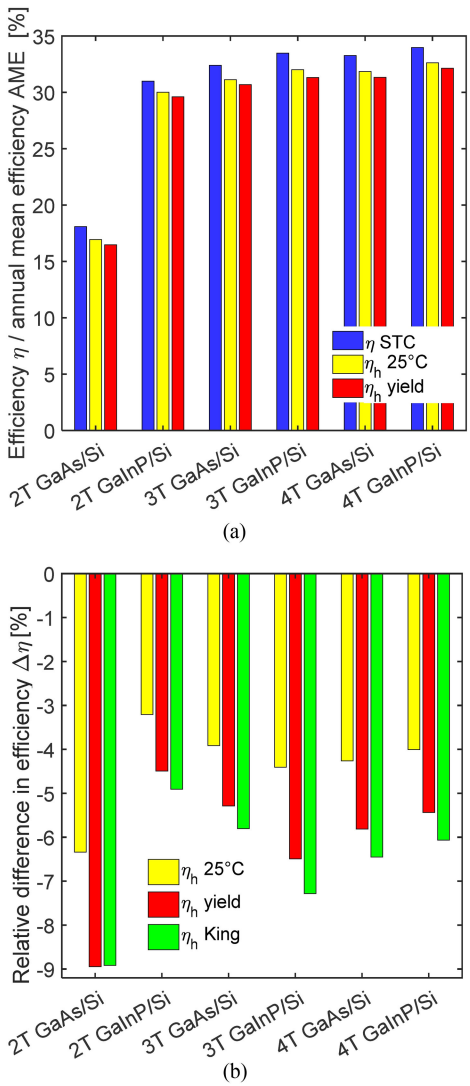

Fig. 4. (a) Efficiencies η of the modeled tandem modules with different terminal configurations under STC in blue and the harvesting efficiency η_h assuming a constant temperature of 25 °C (yellow, η_h 25 °C) or the model of this work (red, η_h yield) (b) shows the relative difference of (a) with respect to the STC η using also the model of King (green, η_h King).

III. Results and Discussion

A. Comparison of Technologies Under STC and Outdoor Conditions

The single top cells reach efficiencies of 20.4% and 26.9% under STC for GaInP and GaAs, respectively. The bottom cell from which we extracted the parameters for the double diode model has an efficiency of 25%. However, please note that this cell was not characterized under the top subcells; therefore we used the EQE data from [1]. Fig. 4(a) shows the efficiency η of the tandem devices under STC in blue and the harvesting efficiency η_h extracted from the energy yield divided by the total insolation (2034 kWh/m²) when assuming the TMY spectra with varying irradiation intensities and spectral composition. For the calculation of the energy yield we use two temperature models: a constant temperature of 25 °C shown in yellow and the temperature calculated according the presented yield model in red.

Under the assumption of equal bottom cells, the 4T GaInP/Si cells reach the highest efficiency of 34.0% and the 4T GaAs/Si cells reach 33.3% under STC. These are slightly higher values than in [1] mainly due to the different bottom cell assumed here. The efficiencies of the 2T devices are substantially lower with 31.0% and 18.1% for GaInP/Si and GaAs/Si devices, respectively. The voltage-matched interconnection (3T) performs similarly well to the 4T configuration under STC; the differences are 1.5%$_{rel}$ and 2.6%$_{rel}$ for GaInP/Si and GaAs/Si, respectively.

Using the same temperature as under STC, i.e., 25 °C, but the TMY spectra of a full year, we find a change in efficiency $\Delta\eta$ of up to 6.3%$_{rel}$ for the 2T GaAs/Si devices [yellow bars in Fig. 4(a) and (b)]. For these devices, the top junction is current limiting when the subcells are series connected and the annual spectrum for Denver shows a blue shift with respect to the AM1.5G spectrum, which increases mismatch loss. In contrast, the top junction is current limiting for 2T GaInP/Si tandem cells resulting in the lowest $\Delta\eta$ of 3.2%$_{rel}$. For the 3T and 4T configurations, the differences are smaller than in the case of the 2T GaAs/Si devices with 3.9%$_{rel}$–4.4%$_{rel}$.

Adding temperature effects using the model of this work [red bars in Fig. 4(a) and (b)] results in additional losses. The largest yield reduction can be observed again for the 2T GaAs/Si devices with an additional reduction of 2.6%$_{rel}$, i.e., in sum of 8.9%$_{rel}$. This is caused on the one hand due to the smaller current temperature coefficient α of the Si bottom subcell, which is filtered under the top subcell, compared to the GaAs top subcell. Thereby, the mismatch is increased further. On the other hand, the low efficiency results in a large amount of P_{loss} and, thus, higher operating temperature. For the GaInP/Si 2T tandem cells, the efficiency is significantly higher, and the top cell limits the current. Thus, the additional loss due to temperature effects is 1.3%$_{rel}$ and smaller compared to the GaAs/Si 2T device.

Similar trends are observed for the voltage matched (3T) case. For the 3T GaInP/Si strings, the voltage at maximum power point V_{mpp} of the individual top cells is more than twice the V_{mpp} of the bottom cells. Since the voltage drop with increasing temperature is larger for the two Si bottom subcells than for the one GaInP top subcell, the mismatch is increased at higher temperature. The additional loss due to thermal effects in the energy yield adds 2.1%$_{rel}$ loss, i.e., in sum 6.5%$_{rel}$ when comparing the STC efficiency and the harvesting efficiency with temperature effects. In the case of the GaAs/Si 3T devices, the top cell limits the voltage, resulting lower additional losses of 1.4%$_{rel}$ and total relative loss of 5.3%$_{rel}$.

For the 4T devices, no matching needs to be taken into account, and thus the additional loss due to thermal losses are similar with 1.4%$_{rel}$ (sum 5.4%$_{rel}$) and 1.6%$_{rel}$ (sum 5.8%$_{rel}$), for the GaInP/Si and GaAs/Si devices, respectively.

Comparing the STC efficiency and the harvesting efficiency with temperature effects for the Si cell alone shows a reduction in efficiency of 7.0%$_{rel}$.There are substantial differences in harvesting efficiency between the use of the implicit solution of our model and if no thermal effects are taken into account. For com-

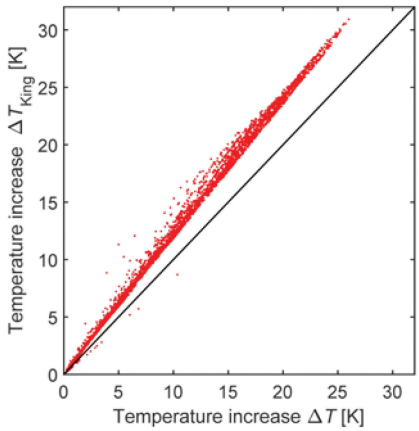

Fig. 5. Comparison of temperature increase above ambient temperature between the model of King and the model of this work for a 4T GaInP/Si device. The solid line is case of equal temperature for both temperature models.

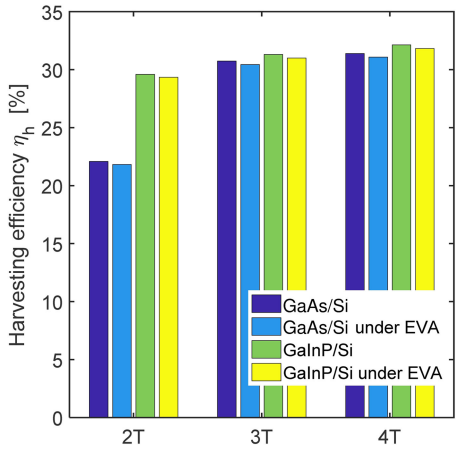

Fig. 6. Harvesting efficiencies of the modeled tandem modules determined from the energy yield divided by the total incoming irradiance for different terminal configurations of GaInP/Si and GaAs/Si devices including luminescent coupling and the spectral of transmittance of an EVA/glass stack (under EVA).

parison, we also performed simulations using the widely used temperature model of King *et al*. [21] as done in other works. Fig. 4(b) shows the relative difference in harvesting efficiency using the King model with respect to the STC efficiency.

In the case of the GaAs/Si 2T devices, the efficiency of the module is similar to those of commercial single junction PV modules due to current mismatch between the cells. Thus, there is no effect due to an increased efficiency and, the temperature model of King and this model differ only by $0.03\%_{rel}$. The deviation of our temperature model from the King model leads to a difference between $-0.5\%_{rel}$ to $-0.8\%_{rel}$ in energy yield for 3T and 4T models. This shows that a model neglecting the module efficiency predicts higher operating temperature and thus lower energy yield. The difference in operation temperatures is as large as 4.9 °C, as shown in Fig. 5, for the case of 4T GaInP/Si device.

This indicates that the STC values provide the correct trends in the final performance of modules, but substantial quantitative differences may occur due to the requirement of current or voltage matching for 2T and 3T devices, respectively.

B. Luminescent Coupling

Luminescent coupling has the potential to increase the current at the maximum power point and thus the energy yield of tandem devices. We use (6) to calculate the current increase using a coupling constant η_{LC} between the two junctions of 0.5, which was measured for good monolithically grown GaInP/GaAs devices [38], as an upper limit for stacked GaAs/Si and GaInP/Si devices.

For the GaInP/Si device, the impact of luminescent coupling is below $0.04\%_{rel}$ in energy yield for 2T, 3T, and 4T devices. In the case of such a 2T device, the top cell is the current-limiting device and the bottom cell operates closer to V_{oc} compared to the case of the independent operation. Photons emitted by the bottom cell are below the bandgap of the top cell and cannot be collected by the top cell. For 3T devices the top subcell's voltage at the independent maximum power point is larger than the maximum power point voltage of the bottom subcell, and thus the top subcell operates closer to I_{sc} compared to the case of the independent operation, and therefore emits almost no photons.

In the case of GaAs/Si 2T devices, there is a yield increase of $34\%_{rel}$ because of the luminescent coupling, since the Si bottom cell is current limiting. Thus, the top cell operates closer to V_{oc} and emits many photons, which are collected with a probability of 0.5 by the bottom cell. The harvesting efficiency increases from $16.5\%_{abs}$ to $22.1\%_{abs}$, which is still well below the Si single-junction efficiency. 3T devices show a slight increase in energy yield of $0.19\%_{rel}$ caused by luminescent coupling. Because of the voltage matching, the top cell will operate at a slightly higher voltage, since it is the voltage-limiting junction in this configuration. For 4T devices, a slight increase of $0.17\%_{rel}$ is calculated.

C. Spectral Effects of EVA Encapsulant

For outdoor operation, PV modules are encapsulated to protect them from the harsh environmental conditions. EVA is the most widely used encapsulant material and for high efficiency tandem devices, the most highly transparent materials will be applied. Therefore, we model the impact of the spectrally resolved absorption simulated from the extinction coefficient by an EVA encapsulant designed for enhanced transmission and a highly transparent low-iron solar glass [37].

Fig. 6 shows the harvesting efficiency of the tandem devices using spectral data and our temperature model, with and without absorption by an EVA layer. Luminescent coupling is taken into account for all configurations. For 3T and 4T devices of both cell types, the energy yields/harvesting efficiencies decrease by $0.98\%_{rel}$–$1.01\%_{rel}$. However, in case of the 2T devices, the harvesting efficiency of the GaInP-based device decreases by $0.86\%_{rel}$, whereas in case of the device with the GaAs top cell, the losses are $1.21\%_{rel}$.

Fig. 7 shows the EQE of the subcells and the absorption by the glass/EVA stack. The III-V semiconductor top cells have a limited blue response for wavelengths smaller than 360 nm,

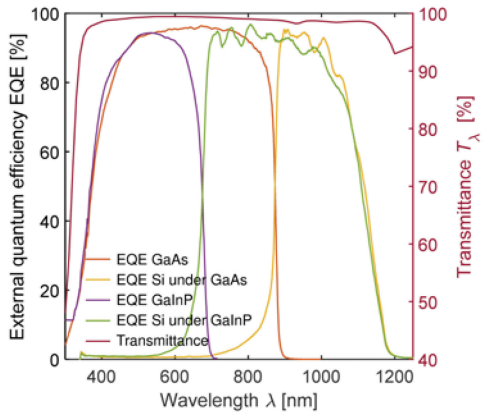

Fig. 7. EQE of the four used subcells from [1] and the transmittance of the simulated EVA/glass stack [37].

so absorption in this range has a minimal impact, but the stack absorbs more light in the near infrared than in the visible range, resulting primarily in a decrease of the bottom cell current. If the bottom cell is the current limiting junction, as in the case of the 2T GaAs/Si devices, the impact of the encapsulant is more pronounced than in the case where the top cell limits the current. Overall, the impact of the EVA is minimal.

IV. Conclusion

We presented a simplified approach to model the energy yield of novel, nonconcentrator tandem devices based on experimental STC *I–V* parameters and the EQE. The application of the model is shown for GaAs and GaInP top subcells on Si bottom subcells. However, the approach can also be used to model the energy yield of other III-V/Si or III-V/III-V tandem configurations, perovskites/Si, or others, for which outdoor performance measurements of modules with similar bottom cell are available.

In general, the STC efficiency correctly predicts relative performance for different tandem cell architectures, but all configurations are expected to produce lower harvesting efficiencies than their STC efficiencies. As shown in other works, the largest effect on the harvesting efficiency of highly efficient III-V/Si tandem cells in Denver, CO, USA, compared to STC efficiency, is the impact of the varying spectra [24]. Assuming the varying outdoor spectra and including the module operating temperature shows that the effect of spectral variations accounts for about 70% and thermal effects for about 30% of the reduction of the harvesting efficiency compared to the STC efficiency. In contrast with this, Liu *et al.* [23], using an analytical temperature model, predicated that thermal effects would dominate for the same location.

The impact of spectral and temperature effects is more pronounced if they increase the current or voltage mismatch. The combination of both aspects results in a reduction of harvesting efficiency compared to the STC efficiency of up to 8.9%$_{\text{rel}}$ for 2T GaAs/Si devices, whereas the loss for GaInP/Si 2T devices is roughly half that with 4.5%$_{\text{rel}}$.

Luminescent coupling has a strong impact for devices with a current-limiting bottom cell as in the case of 2T GaAs/Si tandem devices. There, we observed a relative increase in energy yield of 34%$_{\text{rel}}$, but this device has low overall efficiency. For all other configurations, the effect is below 0.2%$_{\text{rel}}$ and thus can be neglected. The spectral impact of the encapsulation is about 1%$_{\text{rel}}$. We model only slight differences between the investigated configurations for 2T devices, for which it increases or decreases the current mismatch.

For all investigated scenarios, the efficiency of the 2T GaAs/Si reaches up to 22.1% and is thus below the efficiency of the individual sub cells. In contract to this, the 2T GaInP/Si device achieves a harvesting efficiency of 30.0% without encapsulation and thus substantially more than the subcells. This harvesting efficiency is increased by 5.8%$_{\text{rel}}$ to a value of 31.3% for the 3T GaInP/Si configuration and to 32.1% for the 4T case. The relative difference between the harvesting efficiency of the 3T and 4T GaInP/Si configuration is 2.7%$_{\text{rel}}$ when assuming the encapsulation, but only 1.5%$_{\text{rel}}$ under STC. In warmer climates, the difference in the harvesting efficiency between these configurations will increase further and thus might have an impact on decisions about optimizing terminal configurations. The impact of temperature is smallest for the 2T configuration of GaInP/Si devices. For GaAs/Si devices, the difference between the 3T and 4T configurations is 2.7%$_{\text{rel}}$ under STC and 2.1%$_{\text{rel}}$ when assuming spectral and temperature effects and will decrease for warmer locations. Nevertheless, the energy yield for 3T GaAs/Si and GaInP/Si configuration is close to the yield for the 4T devices and outperforms current-matched 2T devices.

Acknowledgment

The authors thank M. Schnabel (NREL), P. Stradins (NREL), E. L. Warren (NREL), M. Vogt (ISFH), M. Köntges (ISFH), R. Peibst (ISFH), S. McAlpine (NREL), and M. Steiner (NREL) for fruitful discussions. The views expressed in the paper do not necessarily represent the views of the DOE or the U.S. Government. The U.S. Government retains and the publisher, by accepting the article for publication, acknowledges that the U.S. Government retains a nonexclusive, paid-up, irrevocable, worldwide license to publish or reproduce the published form of this work, or allow others to do so, for U.S. Government purposes.

References

[1] S. Essig *et al.*, "Raising the one-sun conversion efficiency of III–V/Si solar cells to 32.8% for two junctions and 35.9% for three junctions," *Nat. Energy*, vol. 2, no. 9, 2017, Art. no. 17144.
[2] T. Duong *et al.*, "Rubidium multication perovskite with optimized bandgap for perovskite-silicon tandem with over 26% efficiency," *Adv. Energy Mater.*, vol. 7, no. 14, 2017, Art. no. 1700228.
[3] J. M. Gee, "A comparison of different module configurations for multi-band-gap solar cells," *Solar Cells*, vol. 24, nos. 1/2, pp. 147–155, 1988.
[4] H. Schulte-Huxel, D. J. Friedman, and A. C. Tamboli, "String-level modeling of two, three and four terminal Si-based tandem modules," *IEEE J. Photovoltaics*.
[5] T. Trupke and P. Würfel, "Improved spectral robustness of triple tandem solar cells by combined series/parallel interconnection," *J. Appl. Phys.*, vol. 96, no. 4, 2004, Art. no. 2347.

[6] I. Almansouri, A. Ho-Baillie, S. P. Bremner, and M. A. Green, "Supercharging silicon solar cell performance by means of multijunction concept," *IEEE J. Photovolt.*, vol. 5, no. 3, pp. 968–976, May 2015.
[7] S. Essig *et al.*, "Development of highly-efficient GaInP/Si tandem solar cells," in *Proc. 42nd IEEE Photovolt. Spec. Conf.*, New Orleans, LA, USA, 2015, pp. 1–4.
[8] D. J. Friedman, J. F. Geisz, and M. A. Steiner, "Analysis of multijunction solar cell current–voltage characteristics in the presence of luminescent coupling," *IEEE J. Photovolt.*, vol. 3, no. 4, pp. 1429–1436, Oct. 2013.
[9] Z. Ren *et al.*, "Numerical analysis of radiative recombination and reabsorption in GaAs/Si tandem," *IEEE J. Photovolt.*, vol. 5, no. 4, pp. 1079–1086, Jul. 2015.
[10] E. L. Warren *et al.*, "Maximizing tandem solar cell power extraction using a three-terminal design," *Sustain. Energy Fuels*, vol. 2, pp. 1141–1147, 2018.
[11] M. Rienäcker *et al.*, "Maximum power extraction enabled by monolithic tandems using interdigitated back contact bottom cells with three terminals," *Prog. Photovolt: Res. Appl.*, 2017.
[12] T. Nagashima, K. Okumura, K. Murata, and Y. Kimura, "Three-terminal tandem solar cells with a back-contact type bottom cell," in *Proc. 28th IEEE Photovolt. Spec. Conf.*, Anchorage, AK, USA, 2000, pp. 1193–1196.
[13] J. C. Jimeno *et al.*, "A 3 terminal parallel connected silicon tandem solar cell," *Energy Procedia*, vol. 92, pp. 644–651, 2016.
[14] S. Sakai and M. Umeno, "Theoretical analysis of new wavelength-division solar cells," *J. Appl. Phys.*, vol. 51, no. 9, pp. 5018–5024, 1980.
[15] A. L. Lentine, G. N. Nielson, M. Okandan, J.-L. Cruz-Campa, and A. Tauke-Pedretti, "Enhanced efficiency for voltage matched stacked multijunction cells: Optimization with yearly temperature and spectra variations," in *Proc. 39th IEEE Photovolt. Spec. Conf.*, Tampa, FL, USA, 2013, pp. 788–791.
[16] R. Strandberg, "Spectral and temperature sensitivity of area de-coupled tandem modules," in *Proc. 42nd IEEE Photovolt. Spec. Conf.*, New Orleans, LA, USA, 2015, pp. 1–6.
[17] M. H. Futscher and B. Ehrler, "Modeling the performance limitations and prospects of perovskite/Si tandem solar cells under realistic operating conditions," *ACS Energy Lett.*, vol. 2, no. 9, pp. 2089–2095, 2017.
[18] M. T. Hörantner and H. J. Snaith, "Predicting and optimising the energy yield of perovskite-on-silicon tandem solar cells under real world conditions," *Energy Environ. Sci.*, vol. 10, no. 9, pp. 1983–1993, 2017.
[19] H. Liu *et al.*, "The realistic energy yield potential of GaAs-on-Si tandem solar cells: a theoretical case study," *Opt. Express*, vol. 23, no. 7, pp. A382–A390, 2015.
[20] S. MacAlpine *et al.*, "Simulated potential for enhanced performance of mechanically stacked hybrid III–V/Si tandem photovoltaic modules using DC–DC converters," *J. Photon. Energy*, vol. 7, no. 4, 2017, Art. no. 042501.
[21] D. L. King, W. E. Boyson, and J. A. Kratochvil, "Photovoltaic array performance model," Tech. Rep. SAND2004-3535, Sandia Nat. Lab., Albuquerque, NM, USA, 2004.
[22] B. C. Duck *et al.*, "Energy yield potential of perovskite-silicon tandem devices: 5–10 June 2016," in *Proc. 43rd IEEE Photovolt. Spec. Conf.*, Portland, OR, USA, 2016, pp. 1624–1629.
[23] H. Liu *et al.*, "Predicting the outdoor performance of flat-plate III–V/Si tandem solar cells," *Solar Energy*, vol. 149, pp. 77–84, 2017.
[24] O. Dupré, B. Niesen, S. de Wolf, and C. Ballif, "Field performance versus standard test condition efficiency of tandem solar cells and the singular case of perovskites/silicon devices," *J. Phys. Chem. Lett.*, vol. 9, no. 2, pp. 446–458, 2018.
[25] T. J. Silverman *et al.*, "Reducing operating temperature in photovoltaic modules," *IEEE J. Photovolt.*, vol. 8, no. 2, pp. 532–540, Mar. 2018.
[26] M. R. Vogt *et al.*, "Reduced module operating temperature and increased yield of modules with PERC instead of Al-BSF solar cells," *IEEE J. Photovolt.*, vol. 7, no. 1, pp. 44–50, Jan. 2017.
[27] NREL, National Solar Radiation Database (NSRDB). 2017. [Online] Available: https://maps.nrel.gov/nsrdb-viewer
[28] Sunpower, Datasheet X21-345.
[29] T. J. Silverman *et al.*, "Outdoor performance of a thin-film gallium-arsenide photovoltaic module," in *Proc. 39th IEEE Photovolt. Spec. Conf.*, Tampa, FL, USA, 2013, pp. 103–108.
[30] E. E. Perl *et al.*, "Measurements and modeling of III-V solar cells at high temperatures up to 400 °C," *IEEE J. Photovolt.*, vol. 6, no. 5, pp. 1345–1352, Sep. 2016.
[31] F. Haase *et al.*, "Interdigitated back contact solar cells with polycrystalline silicon on oxide passivating contacts for both polarities," *Jpn. J. Appl. Phys.*, vol. 56, no. 8S2, 2017, Art. no. 08MB15.
[32] O. Dupré, R. Vaillon, and M. A. Green, *Thermal Behavior of Photovoltaic Devices: Physics and Engineering*. Cham, Switzerland: Springer, 2017.
[33] G.-W. Shu *et al.*, "Measuring the junction temperature of GaInP/GaInAs/Ge multijunction solar cells using photoluminescence," *Jpn. J. Appl. Phys.*, vol. 50, no. 9, 2011, Art. no. 92302.
[34] I. Vurgaftman, J. R. Meyer, and L. R. Ram-Mohan, "Band parameters for III–V compound semiconductors and their alloys," *J. Appl. Phys.*, vol. 89, no. 11, pp. 5815–5875, 2001.
[35] V. Alex, S. Finkbeiner, and J. Weber, "Temperature dependence of the indirect energy gap in crystalline silicon," *J. Appl. Phys.*, vol. 79, no. 9, pp. 6943–6946, 1996.
[36] T. Hove, "A method for predicting long-term average performance of photovoltaic systems," *Renew. Energy*, vol. 21, no. 2, pp. 207–229, 2000.
[37] M. R. Vogt, "Development of physical models for the simulation of optical properties of solar cell modules," PhD. dissertation, Leibniz Univ. Hannover, Hannover, Germany, 2015.
[38] M. A. Steiner *et al.*, "Effects of internal luminescence and internal optics on Voc and Jsc of III–V Solar Cells," *IEEE J. Photovolt.*, vol. 3, no. 4, pp. 1437–1442, Oct. 2013.

Authors' photographs and biographies not available at the time of publication.